1-2020

Effects of Thermal Process Parameters on Mechanical Interlayer Strength for Additively Manufactured Ultem 9085

Travis E. Shelton

Zane Wilburn

Carl R. Hartsfield
Air Force Institute of Technology

Gregory R. Cobb

Joshua T. Cerri

See next page for additional authors

Recommended Citation

Shelton, T. E., Willburn, Z. A., Hartsfield, C. R., Cobb, G. R., Cerri, J. T., & Kemnitz, R. A. (2020). Effects of thermal process parameters on mechanical interlayer strength for additively manufactured Ultem 9085. Polymer Testing, 81(January), 106255. https://doi.org/10.1016/j.polymertesting.2019.106255

Polymer Testing 81 (2020) 106255

Contents lists available at ScienceDirect

Polymer Testing

journal homepage: www.elsevier.com/locate/polytest

Material Properties

Effects of thermal process parameters on mechanical interlayer strength for additively manufactured Ultem 9085☆

Travis E. Shelton*, Zane A. Willburn, Carl R. Hartsfield, Gregory R. Cobb, Joshua T. Cerri, Ryan A. Kemnitz

Air Force Institute of Technology, Department of Aeronautics and Astronautics, 2950 Hobson Way, Wright–Patterson Air Force Base, OH 45433-7765, USA

ARTICLE INFO

Keywords:
Additive manufacturing
Adhesion
Fused deposition modeling
Strength
Ultem 9085

ABSTRACT

The effects of the envelope temperature on the microstructure and mechanical strength of Ultem 9085 fused deposition modeling (FDM) components were studied. A customized build chamber was developed for a commercial 3D printer in order to control the envelope temperature during printing. Test specimens were printed in the vertical direction because their mechanical strength exhibited the greatest dependence on inter-layer adhesion and neck development. A delay was introduced between two layers in each specimen in order to create a weak region where the neck was not expected to fully develop. However, none of the specimens failed in this region. Mechanical testing revealed that neck growth was highly dependent on the envelope temperature, and the strength was shown to vary significantly (>20%) based on the envelope temperature. The variability of the mechanical strength also decreased as the envelope temperature increased. Thermal imaging revealed that the cooling rate of the specimens was consistent regardless of the envelope temperature. Fracture analysis confirmed that higher envelope temperatures improved the amount of neck growth and inter-layer adhesion in the specimens. This study showed that increasing the envelope temperature created parts with higher strengths and improved consistencies.

1. Introduction

Ultem 9085 is a polyetherimide thermoplastic with excellent mechanical [1–3] and thermal [4] properties. These rigorous material properties make it a suitable candidate for applications demanding lower mass while still requiring structural strength. Since Ultem 9085 is a thermoplastic, it can be additively manufactured using fused deposition modeling (FDM), a method that creates parts by depositing material one layer at a time through extrusion [5]. During the FDM process, an initial material layer is extruded through a heated nozzle and onto the build plate, and all subsequent layers are deposited on the previous layer [6]. As the material is extruded, it is in a semi-molten state [7], which allows it to fuse to the layer previously deposited. High shear rates of the polymer in the nozzle deform and align the polymer's microstructure [8], and this alignment can affect the diffusive behavior of the printed layer upon the previous layer [9]. Due to this layering approach, there are many parameters that affect the mechanical properties of FDM parts, including the print orientation and the microstructure of the polymer. The mechanical properties can exhibit anisotropic tensile behavior based on the print orientation. The amount of anisotropy exhibited can be minimized through the use of a raster fill. Both Bagsik and Zaldivar demonstrated that specimens in the horizontal direction showed plastic deformation beyond the yield strength, while specimens printed in the vertical direction failed near the yield strength between layers of the print [10,11].

In addition to the print orientation, the thermal environment can affect the material properties of the printed part. The thermal environment includes the temperature of the heating element and the ambient temperature around the printed part, which are known as the model build temperature and the envelope temperature, respectively. The model build temperature can be controlled with software, while the envelope temperature can be directly controlled if the part is printed in a chamber. Both the model build temperature and envelope temperature are important factors of the FDM process that affect the quality of the printed part.

One process controlled by the model build and envelope temperatures is neck development. If a part has enough thermal energy, the roads or layers will begin to fuse upon contact, and a neck will form. Neck growth will then occur based on factors such as the print speed,

☆ The views expressed in this article are those of the authors and do not reflect the official policy or position of the United States Air Force, Department of Defence, or the US government.

* Corresponding author.
E-mail address: travis.shelton@afit.edu (T.E. Shelton).

https://doi.org/10.1016/j.polymertesting.2019.106255
Received 27 September 2019; Received in revised form 20 November 2019; Accepted 23 November 2019
Available online 26 November 2019
0142-9418/Published by Elsevier Ltd.

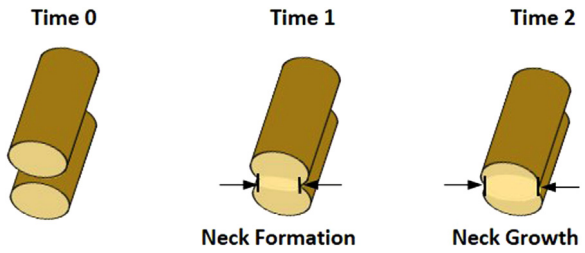

Fig. 1. Kinetics of extruded polymer roads fusing together to form necks.

road diameter, and thermal properties of the printed material. The polymer will then diffuse between the two roads or layers, and they will be fully bonded once the part has cooled [12]. This process is presented as a schematic in Fig. 1. Since the quality of the neck directly influences the mechanical properties of the printed part [12,13], the thermal profile's influence on neck formation must be fully understood.

There have been multiple studies on the effect of the thermal profile on the quality of FDM parts. Bellehemeur et al. [14] created a model that simulated the effect of various process parameters, including the model build and envelope temperatures, on the amount of neck growth that occurred. They found that higher envelope and extrusion temperatures resulted in a larger neck being formed between roads. Faes et al. studied the effects of the cooling time on the inter-layer bonding and mechanical properties of acrylonitrile butadiene styrene (ABS) FDM specimens. They found that increasing the number of printed specimens, which also increased the amount of time that the roads cooled, decreased the ultimate tensile strength (UTS) and elongation at break of the specimens, and reduced the degree of inter-layer bonding. Additionally, they found that the mechanical properties of the specimens exhibited higher degrees of variation that increased with the cooling time. The results of Faes et al. were verified by Morales et al. who studied specimens printed with a set delay between layers to simulate a build with a large number of parts [15]. In addition, they used a thermal camera to determine the cooling rate during the delay time and found that the cooling rate was consistent between specimens. The authors believe that the reduction of the mechanical properties of FDM parts could be mitigated by directly controlling the envelope temperature, and they are unaware of any studies specifically focused on the effects of the envelope temperature on the mechanical properties of Ultem 9085.

This study determines the effect of the thermal profile of the FDM process on the inter-layer bonding of Ultem 9085 parts. Specimens were printed in three orientations on a large-scale 3D printer in order to determine their baseline properties. One of those specimen types was then printed in a customized desktop 3D printer in which the envelope temperature could be directly manipulated. The thermal profile during the printing process was measured by using a microbolometer camera to capture the rates of road cooling changes. Tensile tests were performed on all specimen types to determine their mechanical properties. This research provides further insight into how process parameters can be modified to improve the mechanical properties of Ultem 9085 FDM parts.

2. Methodology

2.1. Baseline tensile specimens

Control tensile specimens were purchased from Stratasys Ltd. in order to obtain baseline material properties for further comparison. The specimens were printed using a Stratasys Fortus 450mc (Stratasys Ltd., Rehovot, Israel). The material studied was 1.75 mm natural color Ultem 9085 (3DXTECH, Grand Rapids, MI, USA). The model build temperature was 375 °C, and the envelope temperature was

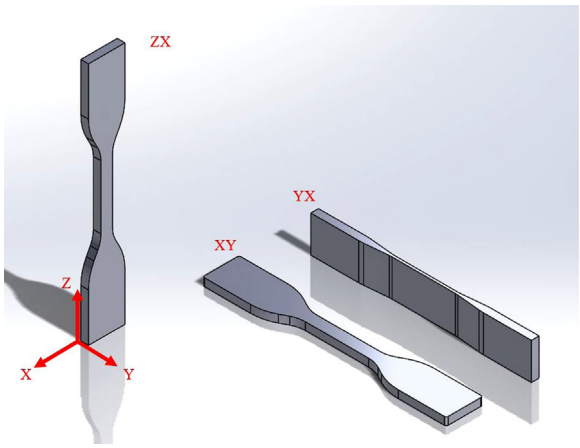

Fig. 2. Print directions used for tensile specimens.

Table 1
Process parameters used to print the inter-layer adhesion specimens in the TAZ 6.

Print parameter	Value
Print speed	40 mm s^{-1}
Infill overlap	15%
Raster angle	±45°
Nozzle diameter	0.4 mm
Nozzle temperature	355 °C
Bed temperature	135 °C

170 °C. Stratasys' default settings for Ultem 9085 were used for all other process parameters. Specimens were printed using three different orientations (see Fig. 2). The YX specimens were Type I dogbone specimens that had modified gage sections and were based on ASTM D638-14 [16], while the XY and ZX specimens were Type IV specimens made using the dimensions listed in ASTM D638-14 [16]. The modified Type I design was used to eliminate the need for support material and better demonstrate how the tensile behavior occurred along roads, since the number of roads in the gage section were greatly reduced. The nominal dimensions of the gage sections are presented in Table 2. Four replicates of each specimen type were printed, which resulted in 15 total specimens.

2.2. Inter-layer adhesion specimens

Since the envelope temperature for the Fortus 450mc was fixed, a separate printer was utilized to study the effects of the envelope temperature on neck development. A chamber with heating lamps and a temperature control mechanism was developed for a LulzBot TAZ 6 3D printer (Aleph Objects, Inc., Loveland, CO, USA). An image of the inside of the chamber with the TAZ 6 is presented in Fig. 3. These specimens were also printed using Ultem 9085. The bulk material was fed directly from a PrintDry filament drying system (Windsor, ON, CA) maintained at 70 °C into the customized TAZ 6. The filament drying system was used to remove excess moisture from the filament, which is known to reduce the material properties of Ultem 9085 [17]. The printer parameters used for the modified TAZ 6 are presented in Table 1. A −150 μm shift was applied to each layer in the Z direction to achieve a negative air gap. A pause was inserted halfway through the specimen, and the specimens' internal temperature was allowed to reach equilibrium with the envelope temperature. The pause was inserted in order to create a region where the inter-layer bonding would be most affected by the envelope temperature, since previous studies have shown that print delays between layers directly affect neck formation [13,15]. Specimens were printed at build volume temperatures of 110 °C, 130 °C, 150 °C, and 170 °C. Five specimens were printed at each build volume temperature, resulting in twenty total specimens.

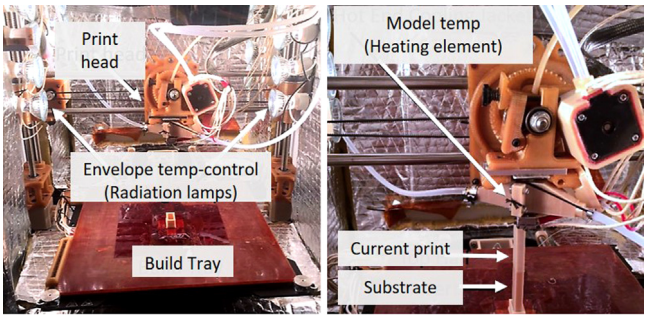

Fig. 3. (a) Image of the TAZ 6 in the customized chamber. (b) Image of a specimen being printed in the customized TAZ 6.

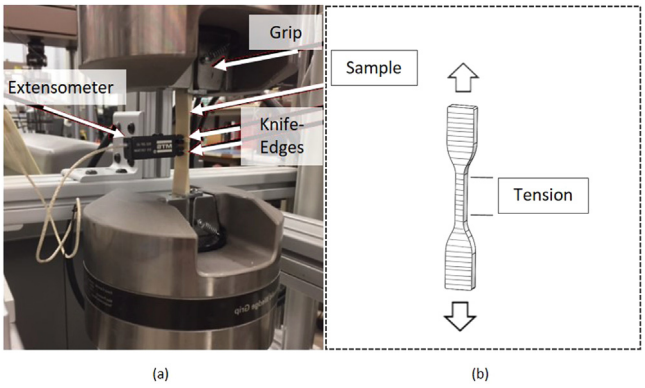

Fig. 4. (a) Mechanical testing setup with (b) the sample loaded in tension.

2.3. Thermal imaging

In-situ thermal images were captured using a FLIR Lepton v1.4 camera (FLIR Systems, Wilsonville, OR, USA) and a Raspberry Pi (Raspberry Pi Foundation, Cambridge, UK). The FLIR image intensity was converted to temperature data by using fourth order scaling. The images were processed in MATLAB (The MathWorks, Inc., Natick, MA, USA) to produce a thermal profile of the specimens. The minimum and maximum temperatures used for calibration in the MATLAB script were the envelope temperature and model build temperature, respectively. The bulk specimen was assumed to be in equilibrium with the envelope temperature while new layers were printed after the pause was introduced. The nozzle was assumed to be at the temperature indicated by the thermistor in the TAZ 6. Images were taken at each layer when the nozzle was equidistant to the specimen and the camera. This ensured that the intensity was properly scaled.

2.4. Mechanical testing

Each tensile specimen was tested using a MTS MTS 810 Servo Hydraulic Machine equipped with an MTS 647 Hydraulic Wedge Grip (MTS Systems Corporation, Eden Prairie, MN, USA). The test setup is presented in Fig. 4. Tabs were mounted to the grip wedges to ensure a uniform grip pressure. An MTS Extensometer, model 632.26F-20, was used to measure changes in the gage section (see Fig. 4a). A 1 mm min^{-1} strain rate was used for all specimens except the Stratasys printed YX specimens, where a strain rate of 5 mm min^{-1} was used. These strain rates were selected to achieve failure between 30 s and 5 min of testing, as ASTM D638-14 states that the speed of testing should rupture the specimen within this time frame [16].

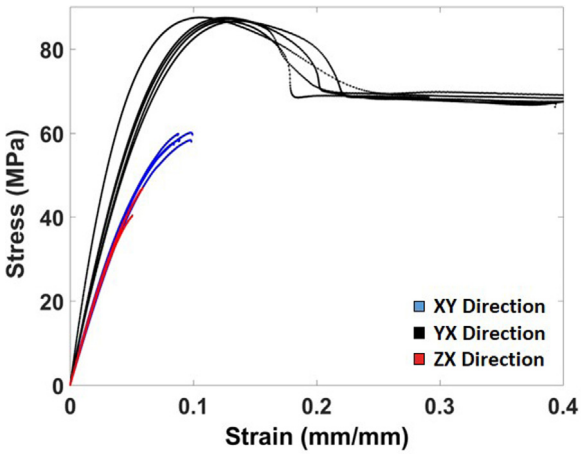

Fig. 5. Stress–strain curves for the baseline specimens.

Table 2
Baseline tensile data for the specimens printed in the Fortus 450mc.

Print direction	XY	YX	ZX
UTS (MPa)	58.9 ± 1.1	87.1 ± 0.4	44.2 ± 3.3
UTS COV (%)	1.83	0.499	7.47
Yield stress (MPa)	29.8 ± 0.7	36.6 ± 3.1	28.3 ± 0.5
Yield stress COV (%)	2.40	8.50	1.62
Elastic modulus (GPa)	1.03 ± 0.04	1.53 ± 0.29	1.03 ± 0.02
Strain-to-Failure (mm mm^{-1})	0.09 ± 0.01	0.42 ± 0.02	0.05 ± 0.01
Gage dimensions (mm x mm)	4 x 6	1 x 19	4 x 6

3. Results

3.1. Baseline mechanical tests

Tensile tests were performed on the specimens printed in the Fortus 450mc in order to collect baseline tensile data and determine which orientation would be most affected by changes in the envelope temperature. Fig. 5 and Table 2 show the results of these tests. Specimens printed in the YX direction had the highest UTS and the largest elastic region. The YX specimens' high UTS and large elastic region can be attributed to the entire gage section consisting of material laid in the direction of tensile force, so the applied force is resisted by strands of material rather than adhesion between roads or layers. There were no significant differences between the elastic region of the XY and ZX specimens. The plastic region of the XY specimens was minimal, while the plastic region of the ZX region was almost negligible. The XY specimens had a higher UTS than the ZX specimens. The YX specimens were the only specimen type that experienced significant plastic deformation before failure occurred. As a result, their strain to failure was much higher than either the XY or ZX specimens.

In order to better understand the failure mechanisms, the fracture sites were analyzed using optical microscopy. These images are presented in Fig. 6. The failure sites show similar trends to the specimens analyzed by Bagsik et al. [10]. The XY specimens (6(a–b)) exhibited brittle failure and failed at the same location in the gage section's contour layer. Since the XY specimens had the largest contour, they also had the greatest cooling time for the nozzle's start–stop position, which created a weak point where failure would occur. The YX specimens (6(c–d)) exhibited brittle failure and clear contour damage. This confirms that the YX specimens' failure was caused by damage to the polymer chains as opposed to damage to the necks between layers. The surface of the ZX specimens was completely smooth (Fig. 6e), which indicates the inter-layer bonds were broken. For this reason, the ZX orientation was chosen for further envelope temperature testing.

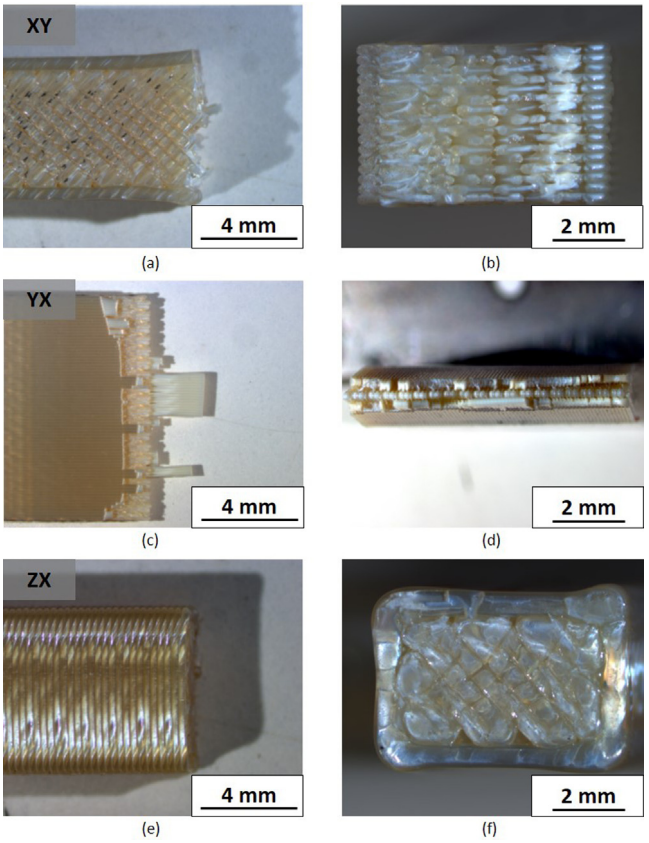

Fig. 6. Fractographs of the baseline tensile specimens. (a) Side and (b) cross sectional view of XY specimen. (c) Side and (d) cross-sectional view of YX specimen. (e) Side and (f) cross-sectional view of ZX specimen.

3.2. Inter-layer adhesion tests

ZX specimens were printed in a modified TAZ 6 printer in order to determine the effect of the thermal profile on the specimens' mechanical properties. As the specimen was printed, a thermal gradient formed between print layers. A schematic of this gradient is presented in Fig. 7a, while an actual thermal image taken during printing is presented in Fig. 7b. Fig. 7b shows that the specimen temperature was highest at the most recent layer, which suggests that it was near the model build temperature, while the temperature of lower layers was near the envelope temperature. As previously stated, the effect of the thermal gradient on neck development between roads was tested by initiating a delay in the gage section. The delay (>5 mins) allowed for specimens' upper most layers to reach equilibrium with the envelope temperature. The delay was expected to create a weak point in the specimens where failure would occur. However, none of the thermal specimens failed at the joint layer.

To understand the thermal environment experienced by the specimens during printing, infrared (IR) imaging was captured at each envelope temperature. Fig. 8a shows the temperature profile as a function of the distance from the nozzle, while Fig. 8b shows a representative thermal profile collected while a 170 °C specimen was printed. Conduction occurred primarily from the nozzle through the specimens. The cooling rate for specimen locations near the nozzle appears to be constant for all specimen types since the slope is consistent in the 0 mm to 10 mm range of the thermal profile presented in Fig. 8a. The 150 °C specimens and 170 °C appeared to reach equilibrium with the envelope temperature near 15 mm from the specimen's top surface, while the 110 °C and 130 °C specimens continued decreasing in temperature within the measured distance (30 mm). The 110 °C and

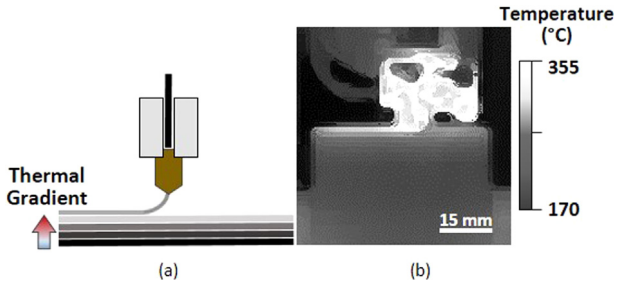

Fig. 7. (a) A schematic showing the thermal gradient observed across print layers. (b) A thermal image of the print head moving from left to right.

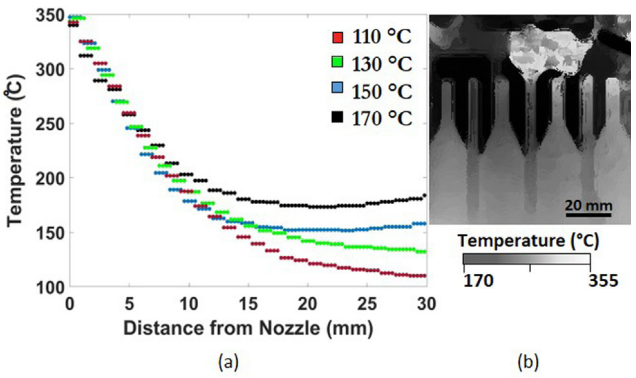

Fig. 8. (a) Experimental thermal profile of the different specimen types. (b) In-situ IR image of the specimen at a build volume temperature of 170 °C.

130° specimens are possibly not reaching equilibrium due to influences on the specimens by the print bed, which is maintained at an average temperature of 135 °C.

Stress–strain curves are presented in Fig. 9a, and mechanical property values calculated from these curves are presented in Table 3. As expected from the results of the baseline ZX specimens, the deformation exhibited by the inter-layer adhesion specimens before failure occurred was almost entirely elastic. The UTS increased as the envelope temperature increased with the exception of specimens printed at 150 °C, and the 170 °C specimens were approximately 20% stronger than the 110 °C specimens (Fig. 9b). However, the UTS of the 170 °C specimens produced in the TAZ 6 did not reach the UTS of the baseline 170 °C specimens. The average UTS of the 170 °C specimens was approximately 13% lower than the UTS of the Fortus 450mc ZX specimens. It is unclear if this is caused by differences in the print parameters or by differences inherent to each system. Additionally, the standard deviations of the UTS decreased as the envelope temperature increased. This suggests that the degree of neck growth increases with the envelope temperature.

While the UTS seems to be directly correlated to the envelope temperature, the 150 °C specimens had a lower average UTS than expected. This discrepancy may simply be due to variability in the print quality at build volume temperatures below 170 °C or caused by residual stresses that only exist when a build volume temperature of 150 °C is used. These residual stresses may mitigate the effects of the improved neck growth on the UTS caused by higher envelope temperatures. Another factor that may have caused residual stresses to form is the time parts were left in the TAZ 6 after manufacturing. This time was inconsistent between builds, and the amount of time the specimens could remain in the printer while the heating elements were still active could be greater than 12 h (i.e., overnight). This extended period in the TAZ 6 could serve as an annealing step because it gives the polymer chains more time to diffuse between roads at an elevated

Table 3
Mechanical properties of inter-layer adhesion specimens.

Build volume temperature (°C)	110	130	150	170
Ultimate strength (MPa)	29.6 ± 3.0	32.7 ± 2.2	30.8 ± 2.3	36.0 ± 0.3
Ultimate strength COV (%)	10.14	6.73	7.47	0.83
Yield stress (MPa)	17.8 ± 10.0	23.5 ± 1.7	24.1 ± 1.7	24.5 ± 1.0
Elastic modulus (GPa)	0.97 ± 0.03	1.02 ± 0.05	0.90 ± 0.03	0.99 ± 0.03
Strain-to-failure (%)	0.035 ± 0.005	0.038 ± 0.004	0.039 ± 0.003	0.042 ± 0.001

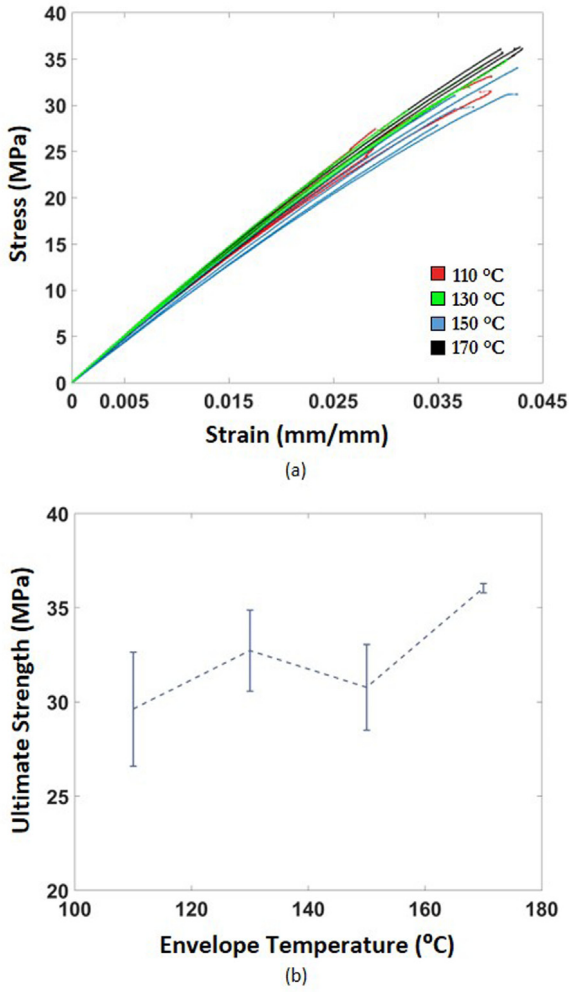

Fig. 9. (a) Stress–strain graph for inter-layer adhesion specimens. (b) UTS as a function of build volume temperature inter-layer adhesion specimens.

temperature [14]. However, further research is required to determine the true cause of this discrepancy.

The elastic modulus and the strain to failure were also calculated for each specimen set (Table 3). While there was slight variability between each specimen, the variability between sets was not statistically significant. This further suggests that differences in the UTS were caused by the degree of neck development between roads and not by other microstructural changes. Unlike the measured UTS, the elastic modulus and strain to failure of the inter-layer adhesion specimens were comparable to the baseline specimens' recorded values.

The 170 °C specimens displayed the most consistent mechanical properties out of the four test specimen sets. The standard deviation of the 170 °C specimens' UTS was an order of magnitude smaller than the other specimens tested, and the coefficient of variability (COV) was reduced by more than 700%. This low variability implies that printing with high envelope temperatures results in FDM Ultem 9085 parts that could be more easily validated for use in advanced applications. Differences in the variability also affect the safety factor that must be considered when deciding how these materials can be implemented into the design of novel components. Increasing the safety factor decreases the maximum load that can be safely applied to a component. If the design strength was based on three standard deviations from the mean, the design strength would be 20.5 MPa and 35.3 MPa for the 110 °C and 170 °C specimens, respectively. These results indicate that higher envelope temperatures lead to parts that have the highest build-to-build consistency.

3.3. Surface analysis

The necking formed across print layers was characterized with a ZEISS LSM 700 laser scanning confocal microscope (Carl Zeiss AG, Oberkochen, Germany). From these scans, an optical profile was measured across print layers as seen in Fig. 10. All of the specimens' profiles contained six distinct layers. The 110 °C specimen exhibited the largest variation in height (236 μm) and had the greatest inconsistencies in their neck formations. The consistency of the 130 °C specimen's layers is improved. However, a large vacancy defect is present on one of its layers (see peak 4 of Fig. 10b). The peaks of the 150 °C specimen appear staggered due to layer-by-layer mismatching. The layer-by-layer mismatching may explain why the UTS of the 150 °C specimens was lower than expected. The height profile of the 170 °C specimen is similar to the 130 °C specimen. However, the valleys of the 170 °C specimens were smoother than the 130 °C specimen, which indicates that the 170 °C specimens had higher degrees of necking. Although increasing the temperature reduced the processing defects, none of the temperatures produced a completely smoothed over surface without layering effects.

Fig. 11 presents the fracture surfaces of representative specimens printed at each envelope temperature. While every specimen failed in a similar manner to the ZX base specimens, the fracture surfaces were inconsistent between specimen sets. The roads of the 110 °C specimens were far more distinct than the other specimens (Fig. 11a). This was most likely due to incomplete neck formation. As the temperature increased, a higher degree of neck growth occurred, and areas where neck formation did not happen became smaller in size and more localized. Individual roads were almost non-existent in the 170 °C specimens, which explained why their UTS was larger and had a smaller standard deviation than the other specimens.

4. Conclusion

The effects of the envelope temperature on the material and mechanical properties of Ultem 9085 FDM components were studied. Initial specimen development on a 3D printer with fixed parameters verified that neck development had the greatest effect on ZX specimens. A customized 3D printer that could control the envelope chamber was successfully developed in order to print four different test specimen cases. Thermal analysis revealed that the specimens cool at a consistent rate regardless of the envelope temperature. Mechanical testing showed that a high degree of neck growth can occur between a newly printed part and a previously printed substrate. This was evident by the fact that the specimens never failed at the layer where a pause was inserted and the specimen was allowed to reach equilibrium with the envelope

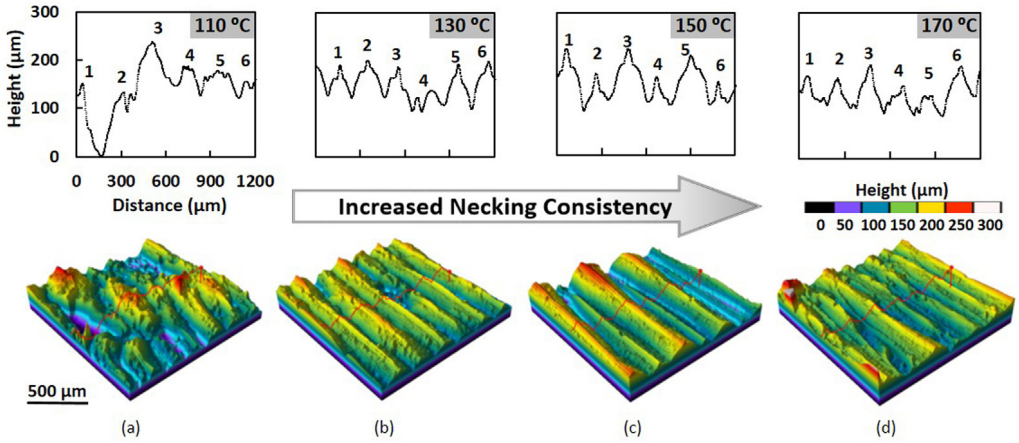

Fig. 10. Surface profiles of the (a) 110 °C, (b) 130 °C, (c) 150 °C, and (d) 170 °C specimens. The layers' periodicity becomes more apparent as seen from the corresponding surface maps.

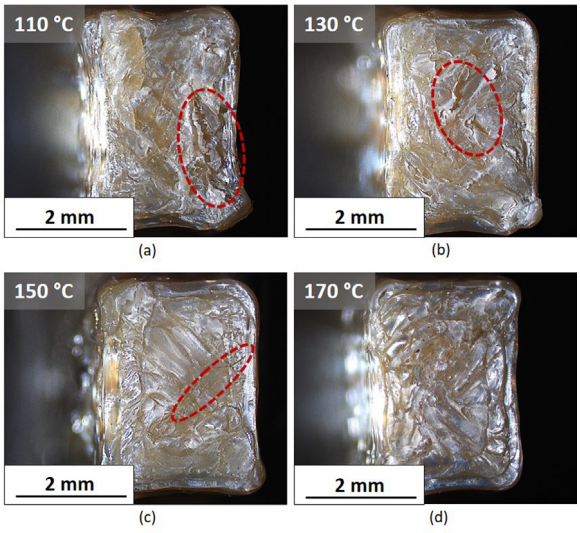

Fig. 11. Cross-sectional views at the point of failure on tensile specimens manufactured in the modified TAZ 6 at the following build volume temperatures: (a) 110 °C, (b) 130 °C, (c) 150 °C, (d) 170 °C. A clean failure between layers can be seen on each specimen pictured.

temperature. The mechanical strength of the specimens was highly dependent on the envelope temperatures, which varied by more than 20% between the 110 °C and 170 °C specimens. The 170 °C specimens also exhibited the lowest amount of variation. Fracture analysis confirmed that neck development increased with the envelope temperature. These results indicate that the envelope temperature does have an effect on the mechanical properties of Ultem 9085 FDM components. This knowledge will be useful when designing Ultem 9085 parts for advanced applications.

Declaration of competing interest

The authors declare that they have no known competing financial interests or personal relationships that could have appeared to influence the work reported in this paper.

CRediT authorship contribution statement

Travis E. Shelton: Conceptualization, Investigation, Supervision, Visualization, Writing — original draft. **Zane A. Willburn:** Data curation, Investigation, Methodology, Writing — original draft. **Carl R. Hartsfield:** Project administration, Resources, Supervision, Validation. **Gregory R. Cobb:** Conceptualization, Writing — review & editing. **Joshua T. Cerri:** Methodology. **Ryan A. Kemnitz:** Resources.

References

[1] A. Bagsik, V. Schöppner, Mechanical properties of fused deposition modeling parts manufactured with ULTEM 9085, in: Proceedings of 69th Annual Technical Conference of the Society of Plastics Engineers, vol. 2, 2011, p. 5.
[2] K.I. Byberg, A.W. Gebisa, H.G. Lemu, Mechanical properties of ULTEM 9085 material processed by fused deposition modeling, Polym. Test. 72 (2018) 335–347, http://dx.doi.org/10.1016/j.polymertesting.2018.10.040.
[3] E. Fox, 3-D Printed Ultem 9085 Testing and Analysis, Tech. Rep., NASA, 2015, URL: https://ntrs.nasa.gov/search.jsp?R=20150017060.
[4] I. Gouzman, E. Grossman, R. Verker, N. Atar, A. Bolker, N. Eliaz, Advances in polyimide-based materials for space applications, Adv. Mater. 31 (18) (2019) 1807738, http://dx.doi.org/10.1002/adma.201807738.
[5] S.H. Ahn, C. Baek, S. Lee, I.S. Ahn, Anisotropic tensile failure model of rapid prototyping parts - fused deposition modeling (FDM), Internat. J. Modern Phys. B 17 (08n09) (2003) 1510–1516, http://dx.doi.org/10.1142/S0217979203019241.
[6] S.-H. Ahn, M. Montero, D. Odell, S. Roundy, P. Wright, Anisotropic material properties of fused deposition modeling ABS, Rapid Prototyp. J. 8 (4) (2002) 248–257.
[7] F. Peng, B.D. Vogt, M. Cakmak, Complex flow and temperature history during melt extrusion in material extrusion additive manufacturing, Addit. Manuf. 22 (2018) 197–206, http://dx.doi.org/10.1016/j.addma.2018.05.015.
[8] C. McIlroy, P. Olmsted, Disentanglement effects on welding behaviour of polymer melts during the fused-filament-fabrication method for additive manufacturing, Polymer 123 (2017) 376–391, http://dx.doi.org/10.1016/j.polymer.2017.06.051.
[9] D. Croccolo, M.D. Agostinis, G. Olmi, Experimental characterization and analytical modelling of the mechanical behaviour of fused deposition processed parts made of ABS-M30, Comput. Mater. Sci. 79 (2013) 506–518, http://dx.doi.org/10.1016/j.commatsci.2013.06.041.
[10] A. Bagsik, V. Schöppner, E. Klemp, FDM part quality manufactured with ULTEM 9085, in: 14th International Scientific Conference on Polymeric Materials, 2010, pp. 1–8.
[11] R.J. Zaldivar, D.B. Witkin, T. Mclouth, D.N. Patel, K. Schmitt, J.P. Nokes, Influence of processing and orientation print effects on the mechanical and thermal behavior of 3D-printed ULTEM® 9085 material, Addit. Manuf. 13 (2017) 71–80, http://dx.doi.org/10.1016/j.addma.2016.11.007.
[12] P.K. Gurrala, S.P. Regalla, Part strength evolution with bonding between filaments in fused deposition modelling, Virtual Phys. Prototyp. 9 (3) (2014) 141–149, http://dx.doi.org/10.1080/17452759.2014.913400.
[13] M. Faes, E. Ferraris, D. Moens, Influence of inter-layer cooling time on the quasi-static properties of ABS components produced via fused deposition modelling, in: 18th CIRP Conference on Electro Physical and Chemical Machining, ISEM XVIII, Procedia CIRP 42 (2016) 748–753, http://dx.doi.org/10.1016/j.procir.2016.02.313.

[14] C. Bellehumeur, L. Li, Modeling of bond formation between polymer filaments in the fused deposition modeling process, J. Manuf. Process. 6 (2) (2004) 170–178, http://dx.doi.org/10.1016/S1526-6125(04)70071-7.

[15] N.G. Morales, T.J. Fleck, J.F. Rhoads, The effect of interlayer cooling on the mechanical properties of components printed via fused deposition, Addit. Manuf. 24 (2018) 243–248, http://dx.doi.org/10.1016/j.addma.2018.09.001.

[16] ASTM International, ASTM D638-14 standard test method for tensile properties of plastics, vol. D638-14, 2014, http://dx.doi.org/10.1520/D0638-14.

[17] R.J. Zaldivar, T.D. Mclouth, G.L. Ferrelli, D.N. Patel, A.R. Hopkins, D. Witkin, Effect of initial filament moisture content on the microstructure and mechanical performance of ULTEM® 9085 3D printed parts, Addit. Manuf. 24 (2018) 457–466, http://dx.doi.org/10.1016/j.addma.2018.10.022.